

## Patterns and dynamics in transitional plane Couette flow

Laurette S. Tuckerman<sup>1,a)</sup> and Dwight Barkley<sup>2,1,b)</sup>

<sup>1</sup>*PMMH (UMR 7636 CNRS-ESPCI-UPMC Paris 6-UPD Paris 7), 10 rue Vauquelin, 75005 Paris, France*

<sup>2</sup>*Mathematics Institute, University of Warwick, Coventry CV4 7AL, United Kingdom*

(Received 4 January 2011; accepted 22 March 2011; published online 19 April 2011)

Near transition, plane Couette flow takes the form of large-scale, oblique, and statistically steady alternating bands of turbulent and laminar flow. Properties of these flows are investigated using direct numerical simulation in a tilted computational domain. Four regimes—uniform, intermittent, periodic, and localized—are characterized. The Fourier spectrum along the direction of variation of the pattern is presented, and the component corresponding to the pattern wavenumber is investigated as an order parameter. The mean flow of a periodic pattern is characterized and shown to lead to a relation between the Reynolds number and the wavelength and angle of a pattern. © 2011 American Institute of Physics. [doi:10.1063/1.3580263]

### I. INTRODUCTION

Transition to turbulence in wall-bounded shear flows has attracted the attention of a large number of researchers using a range of approaches. The three classic wall-bounded shear flows are plane Couette, plane Poiseuille, and pipe flow. This list can be broadened to include counter-rotating Taylor–Couette flow, boundary layer flow, and the flow between differentially rotating disks. The classic tool of linear stability analysis is not useful under these circumstances since the transition to turbulence takes place far from any linear instability.

Transitional flows contain turbulent regions, called spots, slugs, puffs, and bands, which coexist with laminar regions. This leads to questions concerning sizes or wavelengths and growth or decay. A particular coexistence regime consists of alternating turbulent and laminar bands. Both the wavelength and the angle between the bands and the streamwise direction are well-defined and depend on the Reynolds number. The discovery of regular turbulent-laminar patterns dates from about 2000 by Prigent and Dauchot<sup>1–4</sup> in counter-rotating Taylor–Couette flow, although more irregular versions were observed as early as the 1960s by Coles<sup>5</sup> and Van Atta<sup>6</sup> and later by Andereck *et al.*,<sup>7</sup> Hegseth *et al.*,<sup>8</sup> and Goharzadeh and Mutabazi.<sup>9</sup> Turbulent-laminar banded patterns were subsequently observed in experiments on plane Couette flow<sup>1–4</sup> and rotor-stator flow,<sup>10</sup> and in numerical simulations of plane Couette flow,<sup>11–19</sup> of plane Poiseuille flow,<sup>20,21</sup> and of counter-rotating Taylor–Couette flow.<sup>22–24</sup>

We have studied various aspects of turbulent-laminar banded patterns in plane Couette flow by simulating the Navier–Stokes equations in a rectangular computational box, aligned with the direction of the pattern wavevector. This article summarizes what we have learned about these remarkable flows.

### II. GEOMETRY AND COMPUTATIONS

Figure 1 shows a visualization of one of our computed

turbulent-laminar banded patterns at a Reynolds number of 350, more specifically the kinetic energy halfway between the two bounding plates. The small-scale structure seen in Fig. 1 within the turbulent bands is a manifestation of the streamwise vortices and streaks that comprise turbulence in wall-bounded shear flow.<sup>25–27</sup> Figure 2, a spatiotemporal diagram of the variation of the streamwise velocity along the spanwise direction, shows both the dynamic nature of small-scale spatial and temporal features as well as the long-lived nature of the large-scale banded structure. In Fig. 1, the distance between successive turbulent bands is  $\lambda=40$ , and the angle between the bands and the streamwise direction is  $\theta=24^\circ$ , approximately as found in experiment. This angle is actually imposed by our calculation, as we now describe.

The distance between bands is very large compared to the small-scale variation within the bands, and so we choose our domain to be long in the direction of the pattern

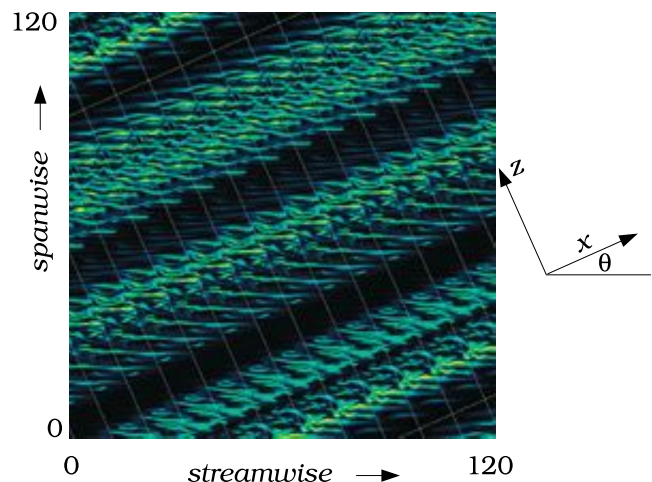


FIG. 1. (Color online) Computed turbulent-laminar pattern at  $Re=350$ . Shown is the kinetic energy at  $y=0$ , midway between bounding plates at  $y=\pm 1$  which move to the right and left in the streamwise direction. Turbulent bands consist of streamwise streaks and vortices. The bands are oriented in the direction denoted by  $x$  at an angle of  $24^\circ$  from the streamwise direction, and are separated by a wavelength of 40 in the direction of the pattern wavevector, denoted by  $z$ .

<sup>a)</sup>Electronic mail: laurette@pmmh.espci.fr.

<sup>b)</sup>Electronic mail: d.barkley@warwick.ac.uk.

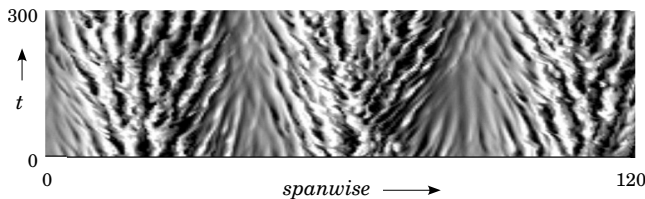


FIG. 2. Streamwise velocity along a line oriented in the spanwise direction in the midplane at  $Re=350$ . Streaks move out from the center of the turbulent region toward the laminar regions. The flow is the same as that in Fig. 1.

wavevector and short in the direction parallel to the bands. That is, our computational domain is rectangular, but tilted with respect to the streamwise and spanwise directions. Figure 1 has been constructed by filling a square oriented along the streamwise-spanwise axes with multiple copies of our tilted rectangular computational domain. Although our computational domain effectively imposes the angle, the wavelength may be any divisor of the domain length in the direction of the pattern wavevector. We call the directions parallel to the bands and to the expected pattern wavevector  $x$  and  $z$ , respectively, with lengths  $L_x$  and  $L_z$ . Our other definitions are conventional:  $y$  is the cross-channel direction, with  $L_y$  taken to be 2. Thus, laminar Couette flow between plates translating in opposite directions and located at  $y = \pm 1$  is

$$\mathbf{U}_{\text{Cou}} = y(\cos \theta \mathbf{e}_x + \sin \theta \mathbf{e}_z), \quad (1)$$

which, just as in the conventional orientation, is trivially a zero-pressure-gradient solution to the Navier–Stokes equations since

$$(\mathbf{U}_{\text{Cou}} \cdot \nabla) \mathbf{U}_{\text{Cou}} = 0 = \nabla^2 \mathbf{U}_{\text{Cou}}. \quad (2)$$

We either take  $L_z$  to be  $\lambda=40$ , the pattern wavelength, or to be  $3\lambda=120$ . The length  $L_x$  is chosen to satisfy a geometric constraint based on the streamwise vortices and streaks that maintain turbulence.<sup>25–27</sup> Near threshold, these vortices and streaks have a spanwise wavelength of  $2L_y \approx 4$ . To accommodate an integer number of these requires  $L_x \sin \theta \approx 4$ .

To solve the Navier–Stokes equations, our computations use Prism,<sup>28</sup> in which the  $(x, y)$  plane is discretized by spectral elements and the  $z$  direction by Fourier modes. The code is parallelized across the Fourier direction. Periodic boundary conditions are imposed in the  $x$  and  $z$  directions, and no-slip boundary conditions in the  $y$  direction. Typical computations use  $N_x \times N_y \times N_z = 81 \times 41 \times 512 = 1.7 \times 10^6$  points or modes to resolve a domain of size  $L_x \times L_y \times L_z = 10 \times 2 \times 40$  and  $N_x \times N_y \times N_z = 61 \times 31 \times 1024 = 1.9 \times 10^6$  points or modes for domains with  $L_x \times L_y \times L_z = 10 \times 2 \times 120$ .

### III. FOUR REGIMES

Our numerical computations, like the physical experiments, are conducted by lowering the Reynolds number. Figures 3 and 4 are spatiotemporal diagrams, taken along the line  $x=y=0$ , where the velocity is zero for laminar plane Couette flow (1). We show timeseries of the spanwise velocity at 32 equally spaced points in the  $z$  direction for a simulation in a domain of size  $L_z=120$ ,  $L_x=10$  as the Reynolds

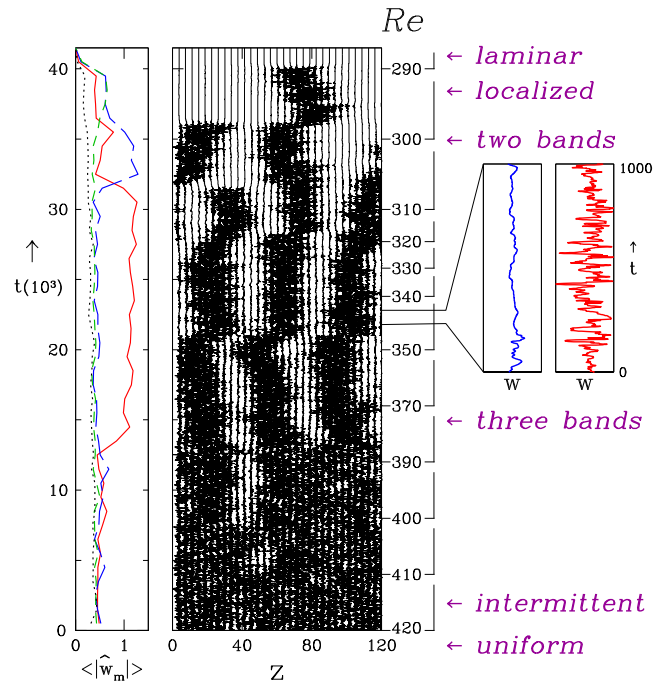


FIG. 3. (Color online) Timeseries in domain with  $L_z=120$ . Middle: spanwise velocity at 32 points along a line in the midplane  $x=y=0$  as the Reynolds number is decreased. Left: modulus of Fourier transform in the  $z$  direction, averaged over time windows of length  $\Delta T=1000$ , showing evolution of components corresponding to wavelengths of 40 (solid red), 60 (long-dashed blue), 120 (short-dashed green), and  $\infty$  (dotted black). Right: evolution of spanwise velocity within laminar (left) and turbulent (right) bands over interval of length  $\Delta T=1000$ . Transition to an intermittent regime is seen at  $Re=410$ , to three bands at  $Re=390$ , to two bands at  $Re=310$ , to a localized state at  $Re=300$ , and to laminar Couette flow at  $Re=290$ .

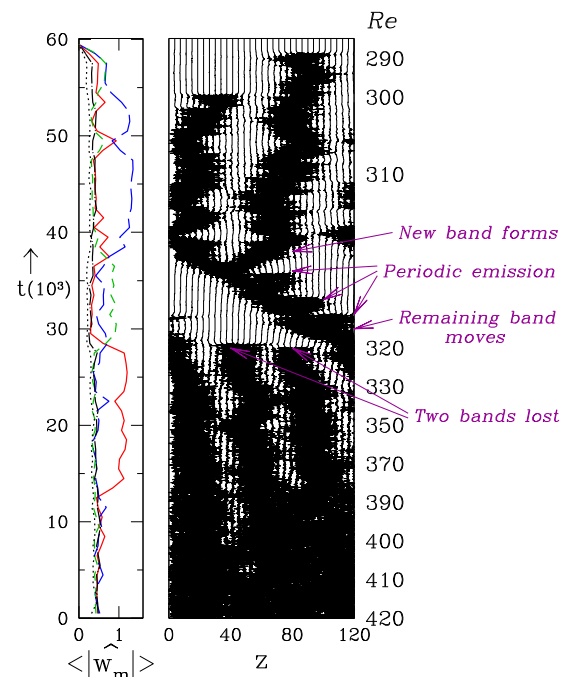


FIG. 4. (Color online) As in Fig. 3, but with slightly different Reynolds number history. Two turbulent bands disappear at  $Re=320$ , leading to translation of the single remaining band with the eventual reappearance of a stationary pattern with two bands.

number is lowered in discrete steps. The accompanying graph along the left shows the moderate-time ( $\Delta T=1000$ ) average of the first Fourier components  $m=0,1,2,3$  (i.e., wavelengths  $\infty, 120, 60$ , and  $40$ ) in the  $z$ -direction. The insets on the right show expanded versions of portions of the timeseries for  $z$  locations in the laminar and the turbulent regions. The terms “turbulent” and “laminar” can be taken here to mean strongly and weakly chaotic, respectively. That is, the turbulent region does not display a Kolmogorov spectrum and the laminar region is not described by the linear plane Couette profile, as shown by the expanded timeseries in Fig. 3. Figure 2 illustrates the detailed behavior of the flow within the two regions.

We define four turbulent patterned regimes, which we call uniform, intermittent, periodic, and localized, listed in order of decreasing Reynolds number. (i) In the uniform regime, turbulence extends across the entire domain, whereas (ii) in the intermittent regime, laminar patches appear and disappear. (iii) In the periodic regime, laminar and turbulent regions are permanent. Although there is small-scale stochastic motion, large-scale motion of the bands is slow or absent. The spatial periodicity is well-defined. (iv) In the localized regime, a single turbulent region is surrounded by laminar flow. In this case, the turbulent region is exponentially localized in space and the laminar region is in fact described by the linear plane Couette profile.

We point out some particular events that can be seen in Fig. 3. At  $Re=310$ , the number of turbulent bands is reduced from three to two; simultaneously the Fourier component corresponding to wavelength 40 is succeeded by that of wavelength 60. At  $Re=300$ , the number of bands is further reduced to one. However, this is not a manifestation of a periodic pattern with wavelength 120, but a localized state, in which the turbulent region can be surrounded by a laminar region of any width. This is demonstrated<sup>11</sup> by producing a pattern containing a single turbulent band of the same width in domains varying from  $L_z=30$  to  $L_z=120$ . Correspondingly, no single Fourier component dominates in this regime. In Fig. 4, two turbulent bands disappear at  $Re=320$ , whereupon the single remaining band moves leftward, periodically emitting the root of a turbulent band. Eventually, one of these succeeds and a stationary pattern with two bands is established. At  $Re=300$ , the number of bands is further reduced to one, and finally below  $Re=290$  only the laminar state remains.

The formation process of turbulent-laminar banded patterns in a large-aspect-ratio domain with streamwise and spanwise extents of  $L_{str}=800$  and  $L_{span}=356$ , in which the orientation of the turbulent bands arises out of initial conditions, is well documented by Duguet *et al.*<sup>16</sup> Competition between patterns with different wavelengths or orientations is characterized by Prigent *et al.*<sup>1-4</sup> and by Rolland and Manneville.<sup>18</sup>

#### IV. TRANSITION BETWEEN UNIFORM, INTERMITTENT, AND PERIODIC PATTERNS

As shown in Figs. 3 and 4, the Fourier transform in the  $z$  direction provides a good quantitative measure for distin-

guishing between the different turbulent-laminar patterns. In this section we present simulations carried out in a domain of length  $L_z=40$ , just large enough to accommodate a single wavelength, for fixed Reynolds numbers.

Figure 5 shows timeseries and spectra for simulations carried out over 20 000 time units at Reynolds numbers of 350, 410, and 500. The first row presents spatiotemporal diagrams like those in Figs. 3 and 4 of the spanwise velocity along a line in the  $z$  direction in the midplane. The next row presents Fourier transforms in the  $z$  direction of this spanwise velocity. These differ from those included in Figs. 3 and 4 as follows. First, we show the square modulus of the entire spectrum, rather than the first few components. Second, we average the instantaneous Fourier components over the entire simulation, rather than over intervals on the order of 100. The peak at  $m=1$ , i.e., at a wavelength of 40, corresponds to the turbulent-laminar pattern, most prominent at  $Re=350$ , reduced at 410 and barely present at 500. This component is plotted as a function of  $Re$  in Fig. 6.

The last row of Fig. 5 shows the spectrum of the streamwise velocity. The  $m=1$  component is still very prominent at  $Re=350$  and 410, but there are additional peaks at  $7 \leq m \leq 11$  for all three Reynolds numbers. These components reflect the small-scale structure seen in Figs. 1 and 2. At these Reynolds numbers, a streamwise vortex occupies approximately the entire gap ( $L_y=2$ ) with an equal spanwise extent, leading to a pair of vortices whose spanwise width is 4, with an extension in the  $z$  direction of  $2 \times L_y / \cos(\theta) = 4 / \cos(24^\circ) = 4.38$ , or a Fourier component of  $40 / 4.38 = 9.1$ . The streamwise vortices in turn lead to streaks, meaning that they advect high and low streamwise velocity toward the midplane from near the bounding plates. The absence of peaks corresponding to small-scale structure in the spanwise spectrum confirms this heuristic picture: while a streamwise vortex should have substantial spanwise velocity, the corresponding velocity in the midplane should be primarily in the  $y$  direction.

We return to the  $m=1$  Fourier component of the spanwise velocity and now consider the probability distribution of its instantaneous values. The Fourier component has both an amplitude  $a$  and a phase  $\phi$ , but, by translational symmetry, its probability distribution  $\rho$  must be independent of phase, i.e., of the location along the  $z$  axis. We write

$$1 = \int_0^\infty da a \underbrace{\int_0^{2\pi} d\phi \rho(a, \phi)}_{p(a)}. \quad (3)$$

We estimate  $p(a_i)$  via

$$p(a_i) \approx \frac{1}{a_i \Delta a} \int_{a_i - \Delta a/2}^{a_i + \Delta a/2} da a \int_0^{2\pi} d\phi \rho(a, \phi), \quad (4)$$

where the integral in Eq. (4) is estimated by counting the proportion of values of  $a$  falling within each of 20 bins of width  $\Delta a$  centered on  $a_i$ .

Figure 7 shows  $p(a)$  obtained from timeseries for  $Re=350, 410$ , and 500 on a logarithmic scale, along with fits of

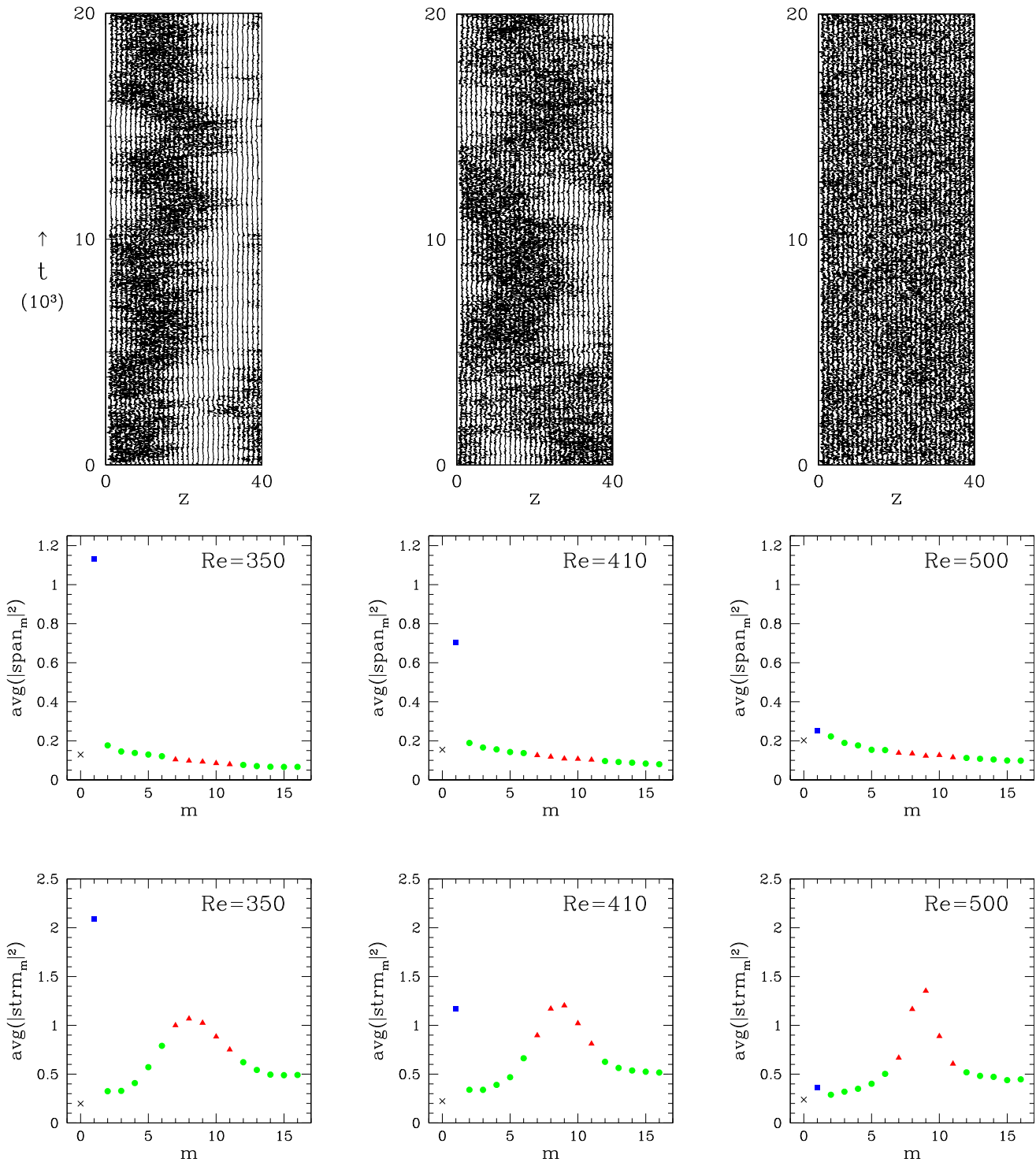


FIG. 5. (Color online) Left column: statistically steady turbulent-laminar pattern at  $Re=350$ . Middle column: intermittent state at  $Re=410$ . Right column: uniform turbulence at  $Re=500$ . Top row: timeseries of the spanwise velocity along the line  $x=y=0$  at 32 equally spaced values of  $z$ . Middle row: time-average of the power spectrum in  $z$  of the spanwise velocity. Bottom row: time-average of the power spectrum of the streamwise velocity. The blue square at  $m=1$  corresponds to the pattern wavelength of 40. The red triangles at  $7 \leq m \leq 11$  correspond to streamwise streaks. The  $m=0$  component is shown as a black cross and the remaining components are shown as green dots.

In  $p(a)$  to even polynomials. At  $Re=500$ , when the turbulence is uniform,  $p(a)$  has a clear maximum at  $a=0$ ; it is in fact extremely well fit by a Gaussian

$$\ln p(a) = c_0 + c_2 a^2. \tag{5}$$

The probability distribution function is almost identical for  $500 \leq Re \leq 600$ .<sup>29</sup> The most probable value shifts from 0 to

positive  $a$  as  $Re$  is lowered, attaining values near 1 (on an arbitrary scale) for  $Re=350$ . We generalize Eq. (5) to a quartic polynomial

$$\ln p(a) = c_0 + c_2 a^2 + c_4 a^4. \tag{6}$$

In the usual scenario for phase transitions,  $c_4$  would vary little with  $Re$  while  $c_2$  would change sign at the transition.

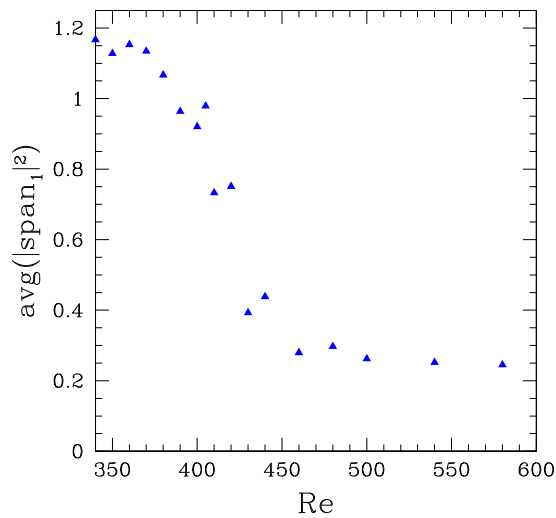


FIG. 6. (Color online) Square modulus of Fourier component corresponding to pattern wavelength as a function of Reynolds number.

However, a quartic polynomial does not provide a good fit for the patterned flows, as exemplified by the curve for  $Re=350$ . Weighting the points by their probability changes the fit, but does not improve it. Figure 8 shows the coefficients of the fit (6) as a function of  $Re$ . The coefficients change very little for  $Re \geq 500$  and within the range  $350 \leq Re \leq 370$ . The coefficients change dramatically within  $410 \leq Re \leq 430$ :  $c_4$  decreases to near zero and  $c_0$  and  $c_2$  exchange signs. The most probable value  $a_{max}$  is difficult to determine at intermediate values because  $p(a)$  is flat and contains noise. Therefore, we take  $a_{max}$  to be the maximum value of the quartic function (6), or 0 if  $|c_4| < 0.1$ , i.e.,

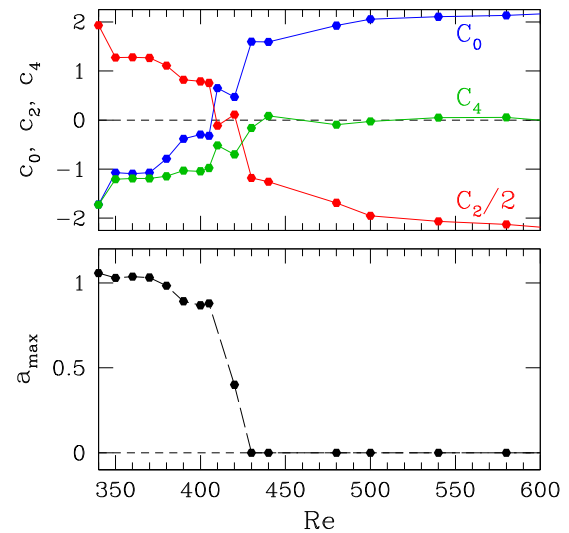


FIG. 8. (Color online) Top: fitting coefficients for quartic functional form (6). Quartic coefficient  $c_4$  becomes negligible for  $Re \geq 430$ , coefficients  $c_0$ ,  $c_2$  change sign near this value as well. Bottom: most probable value of  $a$  is zero for  $Re \geq 430$ .

$$a_{max} = \begin{cases} 0 & \text{if } |c_4| < 0.1 \\ -c_2/2c_4 & \text{otherwise.} \end{cases} \quad (7)$$

Any of these—the amplitude of  $a_{max}$  or  $c_4$  or the sign of  $c_0$ ,  $c_2$ —can be used as an order parameter for the existence of a turbulent-laminar banded pattern.

V. OTHER DOMAINS

Although we have primarily studied the case  $\theta=24^\circ$ , we have also studied other angles. A summary of our results in  $Re$  and  $\theta$  is given in Fig. 9. Figure 10 shows stationary patterned states, some periodic and some localized, with extremal angles and wavelengths at  $Re=350$ . By fixing  $\theta=24^\circ$

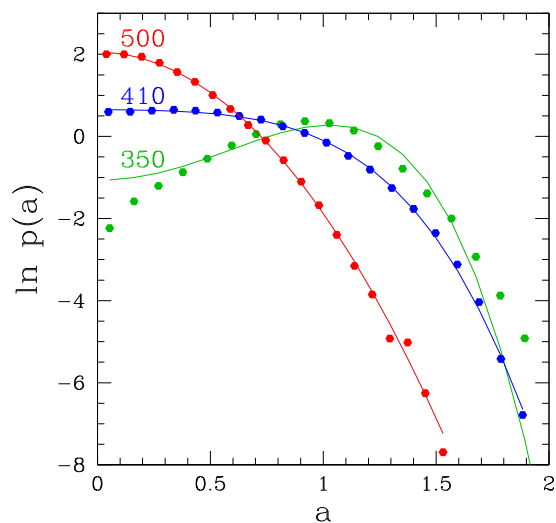


FIG. 7. (Color online) Logarithm  $\ln p(a)$  for the modulus  $a$  of the first Fourier component, for a uniformly turbulent flow at  $Re=500$ , an intermittent flow at  $Re=410$ , and a turbulent-laminar patterned flow at  $Re=350$ . The most probable value is  $a=0$  for uniform turbulence but has a finite value for a patterned flow. Points are obtained by Fourier transforming and binning the data in Fig. 5. Curves are fits to quartic functions.

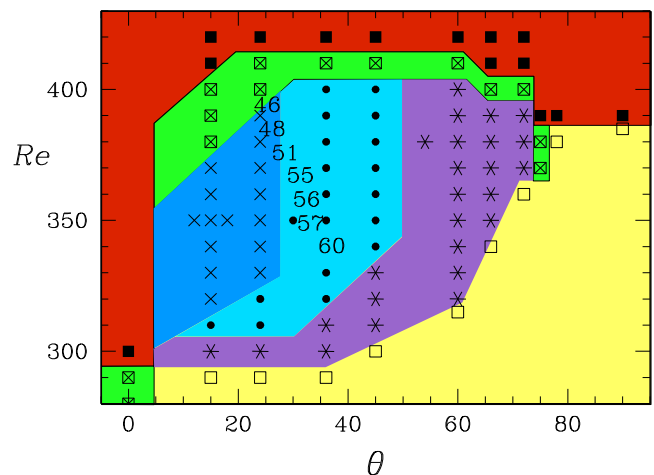


FIG. 9. (Color online) Survey of turbulent-laminar patterned regimes in our computations of plane Couette flow as a function of imposed angle  $\theta$  and Reynolds number  $Re$ . Uniform turbulence (solid squares, red), intermittent (green, crosses in squares), turbulent-laminar patterns with wavelength of 40 (blue, crosses) or 60 (light blue, dots), localized states (stars, purple), laminar Couette flow (hollow squares, yellow). Numbers show wavelengths found in experiments (Ref. 3) at appropriate values of  $\theta$  and  $Re$ .

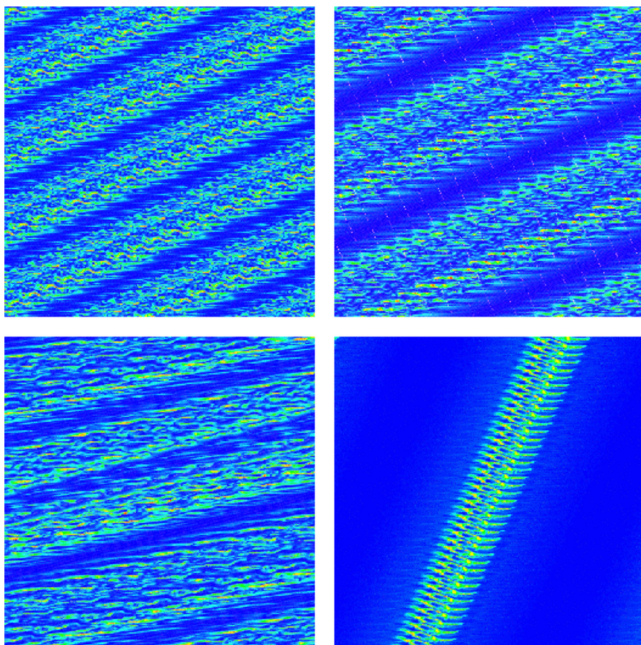


FIG. 10. (Color online) Extremal turbulent-laminar banded patterns at  $Re = 350$ . Top row:  $\theta = 24^\circ$  with  $\lambda = 35$  (left) and  $\lambda = 65$  (right). Bottom row:  $\theta = 15^\circ$  and  $\theta = 66^\circ$ .

and  $L_x$ , and varying  $L_z$ , we produced turbulent-banded patterns with wavelengths between 35 and 65. By fixing  $L_z = 120$  and varying  $\theta$  and  $L_x$  according to  $L_x = 4/\sin \theta$ , we were able to produce patterns at angles between  $15^\circ$  and  $66^\circ$ . (The pattern at  $66^\circ$  is a localized state.) We expect most of these states to be unstable in a less restricted domain.

Figures 11 and 12 show simulations at the extremal angles of  $0^\circ$  and  $90^\circ$ , i.e., in more classic rectangular do-

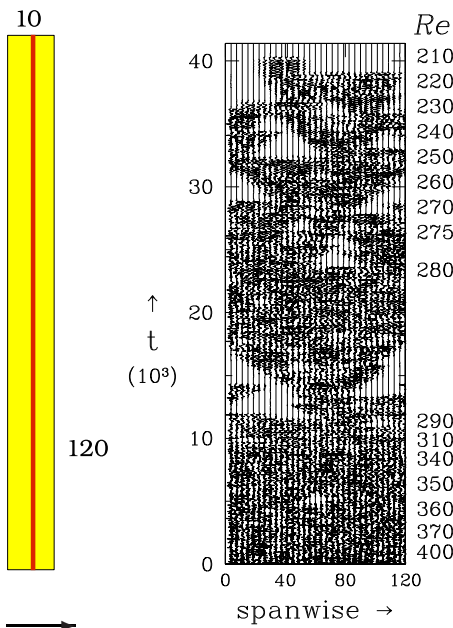


FIG. 11. (Color online) Evolution in a domain with streamwise extent  $L_x = 10$  and spanwise extent  $L_z = 120$ . Timeseries taken at points along long spanwise direction indicated by red line. Turbulent regions subsist far below  $Re = 300$ .

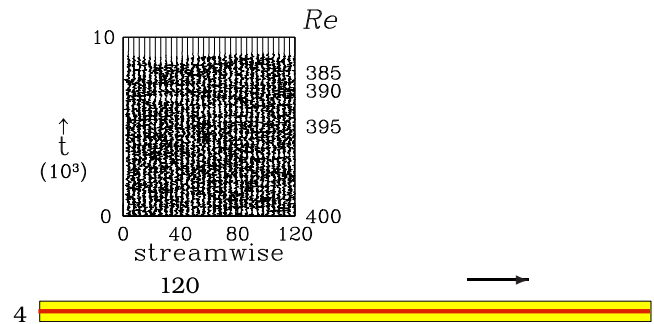


FIG. 12. (Color online) Evolution in a domain with streamwise extent of 120 and spanwise extent of 4. Timeseries taken at points along long streamwise direction indicated by red line. Turbulence disappears throughout the domain for  $Re \leq 385$ .

main aligned with the streamwise and spanwise directions. At  $\theta = 0^\circ$ , the spanwise extent is  $L_z = 120$  and we have fixed the streamwise extent to  $L_x = 10$ . We see that turbulent patches subsist down to  $Re = 220$ , far lower than in the  $\theta = 24^\circ$  case. This is not a well-defined threshold; when simulations are continued at fixed intermediate Reynolds numbers from the intermediate fields in Fig. 11, turbulence persists in some cases and not in others. The Reynolds-number-behavior of the threshold for turbulence is statistical and strongly dependent on the initial condition and the procedure.<sup>30,31</sup> It is also extremely dependent on the dimensions of the domain. In computations of plane Couette flow in a domain similar to that in Fig. 11, Duguet<sup>17</sup> also finds growth of turbulent patches at Reynolds numbers below 300, and suggests that this behavior is a manifestation of the unstable states located on homoclinic snaking branches computed by Schneider *et al.*<sup>32</sup> In contrast, for  $\theta = 90^\circ$ , i.e., in a domain with a long streamwise extent of 120 and short spanwise length of 4, the flow becomes laminar throughout when  $Re \approx 385$  without passing through any intermediate pattern.

### VI. MEAN FLOW OF A PERIODIC TURBULENT-LAMINAR PATTERN

We now analyze in detail the mean flow corresponding to a well-established turbulent-laminar pattern at parameter values  $Re = 350$ ,  $\theta = 24^\circ$ , and  $L_z = 40$  using the data from the timeseries shown in Fig. 5 between  $t = 6000$  and  $t = 8000$ . In this section, we calculate the time-average of the velocity field over the entire domain, rather than just the spanwise velocity at sampled points across a line at the midplane. This time-averaged velocity varies little in  $x$ , the direction parallel to the turbulent bands; it is therefore meaningful to average over  $x$  as well, defining

$$\langle \mathbf{u} \rangle(y, z) \equiv \frac{1}{TL_x} \int_{t=t_0}^{t_0+T} dt \int_{x=0}^{L_x} dx \mathbf{u}(x, y, z, t). \tag{8}$$

The distinctive features of  $\langle \mathbf{u} \rangle = (\langle u \rangle, \langle v \rangle, \langle w \rangle)$  are best viewed by subtracting from it the basic Couette profile (1) and by expressing the flow in the  $(y, z)$  plane via a streamfunction, since  $\partial_y \langle v \rangle + \partial_z \langle w \rangle = 0$ ,

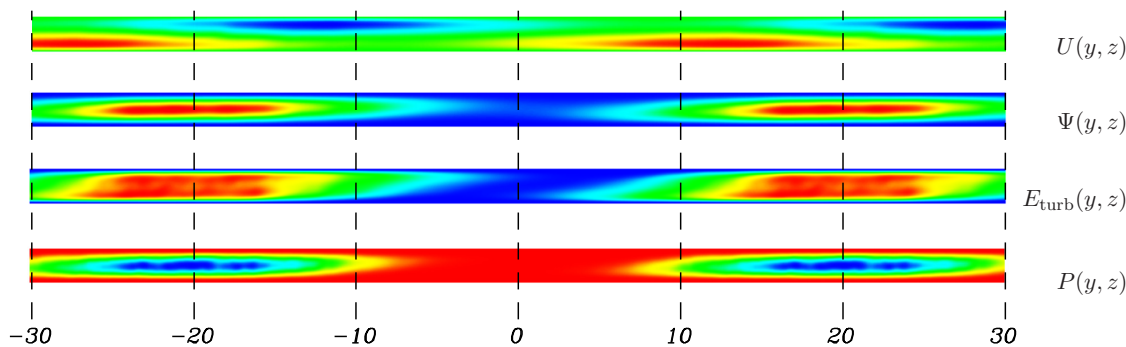


FIG. 13. (Color online)  $U(y,z)$ : transverse component of mean flow.  $\Psi(y,z)$ : streamfunction of in-plane mean flow. A long cell extends from one laminar-turbulent boundary to the other. Gradients of  $\Psi$  are much larger in  $y$  than in  $z$ , i.e.,  $|W| \gg |V|$ . In the laminar region at the center,  $W, V \approx 0$ .  $E_{\text{turb}}(y,z)$ : mean turbulent kinetic energy  $\langle \tilde{\mathbf{u}} \cdot \tilde{\mathbf{u}} \rangle / 2$ . There is a phase difference of  $\lambda_z/4 = 10$  between extrema of  $E_{\text{turb}}$  and  $U$ .  $P(y,z)$ : mean pressure field. Pressure gradients are primarily in the  $y$  direction and within the turbulent region. Color ranges for each field from blue to red:  $U$   $[-0.4, 0.4]$ ,  $\Psi$   $[0, 0.09]$ ,  $E_{\text{turb}}$   $[0, 0.4]$ ,  $P$   $[0, 0.007]$ .

$$\langle \mathbf{u} \rangle = \mathbf{U}_{\text{Cou}} + U \mathbf{e}_x + \nabla \times \psi \mathbf{e}_x. \tag{9}$$

Figure 13 shows  $U$  and  $\psi$  in the  $(y,z)$  plane as well as the turbulent kinetic energy  $\langle \tilde{\mathbf{u}} \cdot \tilde{\mathbf{u}} / 2 \rangle$  and the mean pressure  $\langle p \rangle$ . The fields in Fig. 13 all display centro-symmetry,

$$U(-y, -z) = U(y, z), \tag{10}$$

where  $z=0$  is defined to be at the center of the turbulent region. As was demonstrated in Secs. III and IV, the  $z$  dependence is extremely well approximated by a single Fourier mode. This leads to representations of the form

$$U(y, z) \approx U_0(y) + U_c(y) \cos(2\pi z/\lambda) + U_s(y) \sin(2\pi z/\lambda), \tag{11}$$

involving only three scalar functions  $U_0$ ,  $U_c$ , and  $U_s$ , where  $U_0$ ,  $U_c$  are odd in  $y$  and  $U_s$  is even.

A view of  $\langle \mathbf{u} \rangle$  in two streamwise-spanwise planes at  $y = \pm 0.725$  is shown in Fig. 14. Computations of the mean flow and turbulent kinetic energy for turbulent-laminar banded patterns are presented by Tsukahara *et al.*<sup>21</sup> for plane Poiseuille flow and by Dong<sup>22,23</sup> for Taylor-Couette flow.

The field  $\langle \mathbf{u} \rangle$  obeys the  $(x,t)$ -averaged Navier-Stokes equations whose  $x$  component is

$$0 = \underbrace{-\langle (\mathbf{u} \cdot \nabla) \langle \mathbf{u} \rangle \rangle}_{\text{nonlinear term}} - \underbrace{\langle (\tilde{\mathbf{u}} \cdot \nabla) \tilde{\mathbf{u}} \rangle}_{\text{turbulent forcing}} + \underbrace{\frac{1}{\text{Re}} \nabla^2 \langle \mathbf{u} \rangle}_{\text{viscous term}}, \tag{12}$$

where  $\tilde{\mathbf{u}} \equiv \mathbf{u} - \langle \mathbf{u} \rangle$ . Figure 15 shows the  $x$  components of these forces as a function of  $z$  at  $y=0.725$ . In the laminar regions, the turbulent forcing term is absent. The nonlinear and viscous terms necessarily counterbalance one another; neither one is zero, as would be the case for  $\mathbf{U}_{\text{Cou}}$ . Thus, it is clear that, even in the laminar region,  $\langle \mathbf{u} \rangle \neq \mathbf{U}_{\text{Cou}}$ .

The balance in the laminar region provides a basis for a quantitative relation between  $\theta$ ,  $\text{Re}$ , and  $\lambda$ . Because the wavenumber  $\lambda=40$  is long relative to  $L_y=2$ , the Laplacian is dominated by variation in  $y$ , as in boundary layer theory, and the viscous term is very well approximated by

$$\frac{1}{\text{Re}} \nabla^2 = O\left(\frac{\pi^2}{\text{Re}}\right). \tag{13}$$

The nonlinear term is dominated by advection in the  $z$  direction by  $\mathbf{U}_{\text{Cou}}$ . Evaluating it at a typical value  $y=1/2$ , we obtain as an estimate for the nonlinear term

$$\langle (\mathbf{u} \cdot \nabla) \rangle \approx \mathbf{e}_z \cdot \mathbf{U}_{\text{Cou}} \partial_z \approx \sin \theta y \frac{2\pi}{\lambda} \approx \sin \theta \frac{\pi}{\lambda}. \tag{14}$$

A more complete justification<sup>13</sup> of Eqs. (13) and (14) relies on the full computed fields and the functional form (11). The balance between Eqs. (13) and (14) leads to

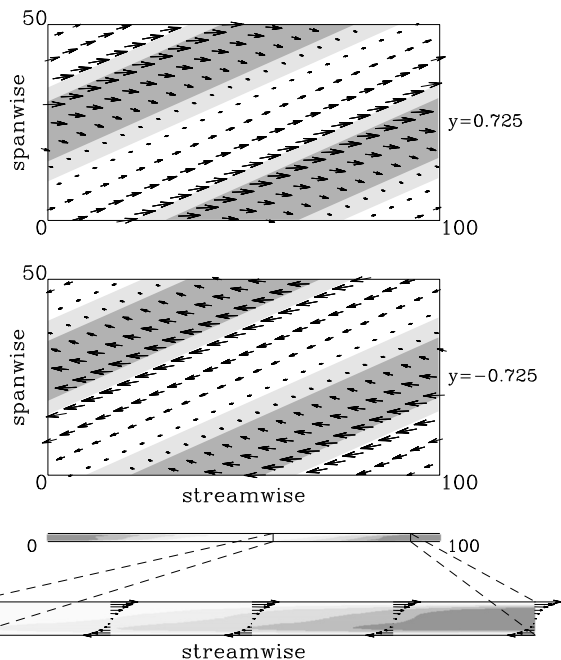


FIG. 14. Mean velocity components seen in three planes with standard orientation for Couette flow. The turbulent regions are shaded. Top: velocity components in the streamwise-spanwise plane at  $y=0.725$  (upper part of the channel). Middle: same except  $y=-0.725$  (lower part of the channel). Bottom: flow in a constant spanwise cut. The mean velocity is shown in the enlarged region.

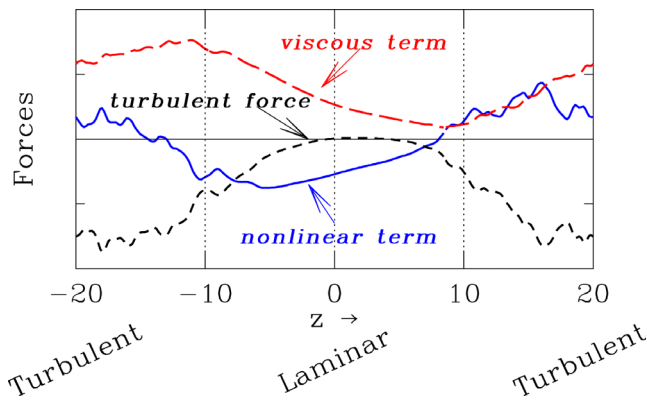


FIG. 15. (Color online) Mean forces in  $x$  direction as a function of  $z$  at  $y=0.725$  for turbulent-laminar pattern at  $Re=350$ . Advective  $-(\mathbf{U} \cdot \nabla)U$  (blue, solid), viscous  $\nabla^2 U/Re$  (red, dashed), and turbulent  $-\langle(\bar{\mathbf{u}} \cdot \nabla)\bar{\mathbf{u}}\rangle$  (black, short-dashed) forces. In the laminar region ( $z \approx 0$ ), the Reynolds-stress force vanishes and the viscous and advective forces are equal and opposite to one another.

$$\frac{Re \sin \theta}{\pi \lambda} = O(1). \quad (15)$$

Equation (15) gives an order-of-magnitude relationship between  $Re$ ,  $\theta$ , and  $\lambda$ , as seen in Fig. 16, which includes experimental and numerical observations of plane Couette, Taylor–Couette, plane Poiseuille, and rotor-stator flow. A uniform definition of Reynolds numbers, angles, and wavelengths for these various flows is based on the average shear.<sup>3,13</sup> For the numerical observations, the angles and wavelengths are highly constrained except in the case of Duguet *et al.*<sup>16</sup>

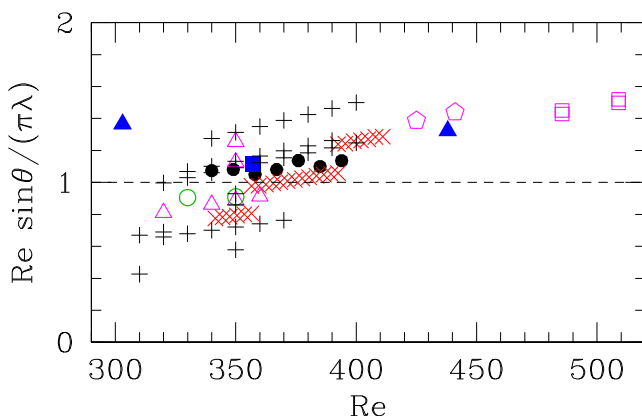


FIG. 16. (Color online)  $Re \sin \theta / (\pi \lambda)$  for turbulent-laminar patterns in experiment and computations in various wall-bounded shear flows. Experimental measurements by Prigent *et al.* (Ref. 3) of plane Couette flow (full black circles) and Taylor–Couette flow (red crosses). Experimental measurements of rotor-stator flow by Cros and Le Gal (Ref. 10) (full blue triangles). Simulations of plane Poiseuille flow by Tsukahara *et al.* (Refs. 20 and 21) (full blue square). Simulations of Taylor–Couette flow by Meseguer *et al.* (Ref. 24) (hollow magenta pentagons) and by Dong (Refs. 22 and 23) (hollow magenta squares). Simulations of plane Couette flow by Duguet (Ref. 16) (hollow green circles), by Philips and Manneville (Ref. 19) (hollow black squares), and by Barkley and Tuckerman (Ref. 13) (black crosses).

## VII. CONCLUSION

Turbulent-laminar patterns are a fascinating feature of many wall-bounded shear flows near transition. We have carried out detailed studies of turbulent-laminar patterns in plane Couette flow. Our main findings are as follows. First, turbulent-laminar banded patterns can be further divided into different regimes—intermittent, periodic, or localized. Second, the Fourier component corresponding to the pattern wavevector (the direction we have called  $z$ ) leads to the appropriate order parameter for describing such patterns. The transition from uniform turbulence to a turbulent-laminar pattern is described by a bifurcation in its probability distribution function. Third, the mean flow associated with a periodic turbulent-laminar pattern consists primarily of flow along the turbulent-laminar boundaries (the direction we have called  $x$ ), maintained by a weaker circulation around the turbulent regions. The mean balance of forces determines the relation between the angle, wavelength, and Reynolds number of the patterns.

It seems plausible that studies of such patterns will lead to insights concerning the cause or nature of the fundamental problem of transition to turbulence. But even in the absence of such results, turbulent-laminar patterns are a perplexing and exotic object of study in their own right.

## ACKNOWLEDGMENTS

The authors thank O. Dauchot, Y. Duguet, P. Manneville, and A. Prigent for helpful discussions. This work was performed using high performance computing resources provided by the Grand Equipement National de Calcul Intensif–Institut du Développement et des Ressources en Informatique Scientifique project 1119. This paper is based on an invited lecture, which was presented by L.S.T. at the 62nd Annual Meeting of the Division of Fluid Dynamics of the American Physical Society, held 22–24 November 2009 in Minneapolis, MN.

<sup>1</sup>A. Prigent, “La spirale turbulente: Motif de grande longueur d’onde dans les écoulements cisailés turbulents,” Ph.D. thesis, University Paris-Sud, 2001.

<sup>2</sup>A. Prigent, G. Gregoire, H. Chaté, O. Dauchot, and W. van Saarloos, “Large-scale finite-wavelength modulation within turbulent shear flows,” *Phys. Rev. Lett.* **89**, 014501 (2002).

<sup>3</sup>A. Prigent, G. Gregoire, H. Chaté, and O. Dauchot, “Long-wavelength modulation of turbulent shear flows,” *Physica D* **174**, 100 (2003).

<sup>4</sup>A. Prigent and O. Dauchot, “Transition to versus from turbulence in subcritical Couette flows,” in *IUTAM Symposium on Laminar-Turbulent Transition and Finite Amplitude Solutions*, edited by T. Mullin and R. Kerswell (Springer, Dordrecht, 2005), pp. 193–217.

<sup>5</sup>D. Coles, “Transition in circular Couette flow,” *J. Fluid Mech.* **21**, 385 (1965).

<sup>6</sup>C. Van Atta, “Exploratory measurements in spiral turbulence,” *J. Fluid Mech.* **25**, 495 (1966).

<sup>7</sup>C. D. Andereck, S. S. Liu, and H. L. Swinney, “Flow regimes in a circular Couette system with independently rotating cylinders,” *J. Fluid Mech.* **164**, 155 (1986).

<sup>8</sup>J. J. Hegseth, C. D. Andereck, F. Hayot, and Y. Pomeau, “Spiral turbulence and phase dynamics,” *Phys. Rev. Lett.* **62**, 257 (1989).

<sup>9</sup>A. Goharzadeh and I. Mutabazi, “Experimental characterization of intermittency regimes in the Couette-Taylor system,” *Eur. Phys. J. B* **19**, 157 (2001).

<sup>10</sup>A. Cros and P. Le Gal, “Spatiotemporal intermittency in the torsional

- Couette flow between a rotating and a stationary disk,” *Phys. Fluids* **14**, 3755 (2002).
- <sup>11</sup>D. Barkley and L. S. Tuckerman, “Computational study of turbulent laminar patterns in Couette flow,” *Phys. Rev. Lett.* **94**, 014502 (2005).
- <sup>12</sup>D. Barkley and L. S. Tuckerman, “Turbulent-laminar patterns in plane Couette flow,” in *IUTAM Symposium on Laminar-Turbulent Transition and Finite Amplitude Solutions*, edited by T. Mullin and R. Kerswell (Springer, Dordrecht, 2005), pp. 107–127.
- <sup>13</sup>D. Barkley and L. S. Tuckerman, “Mean flow of turbulent-laminar patterns in plane Couette flow,” *J. Fluid Mech.* **576**, 109 (2007).
- <sup>14</sup>L. S. Tuckerman, D. Barkley, and O. Dauchot, “Statistical analysis of the transition to turbulent-laminar banded patterns in plane Couette flow,” *J. Phys.: Conf. Ser.* **137**, 012029 (2008).
- <sup>15</sup>L. S. Tuckerman, D. Barkley, and O. Dauchot, “Instability of uniform turbulent plane Couette flow: Spectra, probability distribution functions and  $K-\Omega$  closure model,” in *Seventh IUTAM Symposium on Laminar-Turbulent Transition*, edited by P. Schlatter and D. Henningson (Springer, New York, 2010), Vol. 18, pp. 59–66.
- <sup>16</sup>Y. Duguet, P. Schlatter, and D. S. Henningson, “Formation of turbulent patterns near the onset of transition in plane Couette flow,” *J. Fluid Mech.* **650**, 119 (2010).
- <sup>17</sup>Y. Duguet, O. Le Maître, and P. Schlatter, “Stochastic and deterministic motion of a laminar-turbulent interface in a shear flow” (private communication).
- <sup>18</sup>J. Rolland and P. Manneville, “Pattern fluctuations in transitional plane Couette flow,” *J. Stat. Phys.* **142**, 577 (2011).
- <sup>19</sup>J. Philip and P. Manneville, “From temporal to spatiotemporal dynamics in transitional plane Couette flow,” *Phys. Rev. E* **83**, 036308 (2011).
- <sup>20</sup>T. Tsukahara, Y. Seki, H. Kawamura, and D. Tochio, “DNS of turbulent channel flow at very low Reynolds numbers,” *Proceedings of the Fourth International Symposium on Turbulence and Shear Flow Phenomena*, 2005, pp. 935–940.
- <sup>21</sup>T. Tsukahara, K. Iwamoto, H. Kawamura, and T. Takeda, “DNS of heat transfer in a transitional channel flow accompanied by a turbulent puff-like structure,” in *Proceedings of the Fifth International Symposium on Turbulence, Heat and Mass Transfer*, Dubrovnik, Croatia, 25–29 September 2006, edited by Y. N. K. Hanjalić, Y. Nagano, and S. Jakirlić.
- <sup>22</sup>S. Dong, “Evidence for internal structures of spiral turbulence,” *Phys. Rev. E* **80**, 067301 (2009).
- <sup>23</sup>S. Dong and X. Zheng, “Direct numerical simulation of spiral turbulence,” *J. Fluid Mech.* **668**, 150 (2011).
- <sup>24</sup>A. Meseguer, F. Mellibovsky, M. Avila, and F. Marques, “Instability mechanisms and transition scenarios of spiral turbulence in Taylor-Couette flow,” *Phys. Rev. E* **80**, 046315 (2009).
- <sup>25</sup>J. Jiménez and P. Moin, “The minimal flow unit in near-wall turbulence,” *J. Fluid Mech.* **225**, 213 (1991).
- <sup>26</sup>J. M. Hamilton, J. Kim, and F. Waleffe, “Regeneration mechanisms of near-wall turbulence structures,” *J. Fluid Mech.* **287**, 317 (1995).
- <sup>27</sup>F. Waleffe, “Homotopy of exact coherent structures in plane shear flows,” *Phys. Fluids* **15**, 1517 (2003).
- <sup>28</sup>R. D. Henderson and G. E. Karniadakis, “Unstructured spectral element methods for simulation of turbulent flows,” *J. Comput. Phys.* **122**, 191 (1995).
- <sup>29</sup>L. S. Tuckerman, D. Barkley, O. Moxey, and O. Dauchot, “Order parameter in laminar-turbulent patterns,” in *Advances in Turbulence XII*, Springer Proceedings in Physics Vol. 132, edited by B. Eckhardt (Springer, New York, 2009), pp. 89–91.
- <sup>30</sup>S. Bottin, O. Dauchot, F. Daviaud, and P. Manneville, “Experimental evidence of streamwise vortices as finite amplitude solutions in transitional plane Couette flow,” *Phys. Fluids* **10**, 2597 (1998).
- <sup>31</sup>A. Schmieguel and B. Eckhardt, “Persistent turbulence in annealed plane Couette flow,” *Phys. Fluids* **51**, 395 (2000).
- <sup>32</sup>T. M. Schneider, J. F. Gibson, and J. Burke, “Snakes and ladders: Localized solutions of plane Couette flow,” *Phys. Rev. Lett.* **104**, 104501 (2010).